Antiviral Research 169 (2019) 104557

Contents lists available at ScienceDirect

Antiviral Research

journal homepage: www.elsevier.com/locate/antiviral

BAY 41-4109-mediated aggregation of assembled and misassembled HBV capsids in cells revealed by electron microscopy

Virgile Rat[a], Florian Seigneuret[a], Julien Burlaud-Gaillard[b], Roxane Lemoine[c], Christophe Hourioux[a,b], Fabien Zoulim[d,e,f], Barbara Testoni[d,e,f], Jean-Christophe Meunier[a], Clovis Tauber[g], Philippe Roingeard[a,b], Hugues de Rocquigny[a,*]

[a] Morphogenèse et Antigénicité Du VIH et des Virus des Hépatites, Inserm – U1259 MAVIVH, Université de Tours et CHRU de Tours, 10 Boulevard Tonnellé - BP 3223, 37032, Tours Cedex 1, France
[b] Plate-Forme IBiSA des Microscopies, PPF ASB, Université de Tours and CHRU de Tours, 10 Boulevard Tonnellé - BP 3223, 37032, Tours Cedex 1, France
[c] B-Cell Resources Platform, EA4245 "Transplantation, Immunologie et Inflammation", Université de Tours, 10 Boulevard Tonnellé, 37032, Tours Cedex 1, France
[d] INSERM U1052-Cancer Research Center of Lyon (CRCL), 69008, Lyon, France
[e] University of Lyon, UMR_S1052, CRCL, 69008, Lyon, France
[f] Department of Hepatology, Croix Rousse Hospital, Hospices Civils de Lyon, France
[g] UMRS Inserm U1253 - Université de Tours, 10 Boulevard Tonnellé - BP 3223, 37032, Tours Cedex 1, France

ARTICLE INFO

Keywords:
HBV
Electron microscopy
Aggregation
CAMs
Confocal microscopy
HBc

ABSTRACT

HBc is a small protein essential for the formation of the icosahedral HBV capsid. Its multiple roles in the replication cycle make this protein a promising target for the development of antiviral molecules. Based on the structure of HBc, a series of HBV assembly inhibitors, also known as capsid assembly modulators, were identified. We investigated the effect of BAY 41–4109, a heteroaryldihydropyrimidine derivative that promotes the assembly of a non-capsid polymer. We showed, by confocal microscopy, that BAY 41–4109 mediated HBc aggregation, mostly in the cytoplasm of Huh7 cells. Image analysis revealed that aggregate size depended on BAY 41–4109 concentration and treatment duration. Large aggregates in the vicinity of the nucleus were enclosed by invaginations of the nuclear envelope. This deformation of the nuclear envelope was confirmed by transmission electron microscopy (TEM) and immuno-TEM. These two techniques also revealed that the HBc aggregates were accumulations of capsid-like shells with an electron-dense material consisting of HBV core fragments. These findings, shedding light on the ultrastructural organization of HBc aggregates, provide insight into the mechanisms of action of BAY 41–4109 against HBV and will serve as a basis for comparison with other HBV capsid assembly inhibitors.

1. Introduction

Despite the availability of an efficient vaccine, an estimated 300 million people are living with hepatitis B virus (HBV) infection, which causes~ 900,000 deaths each year, mostly from complications, such as cirrhosis and hepatocellular carcinoma (Neuveut et al., 2010). Antiviral treatments are well tolerated but they cannot cure the infection (Liang et al., 2015).

HBV is an enveloped virus with a 3.2 kb partially double-stranded DNA genome protected by the HBc protein. HBc consists of 183–185 residues, forming two domains (Fig. 1): the N-terminal domain (NTD; residues 1–140), which assembles into a capsid, linked by a flexible linker to the basic C-terminal domain (residues 150–183), which interacts with nucleic acids (Venkatakrishnan and Zlotnick, 2016).

The role of HBc capsid formation and virus replication (Chu et al., 2014; Nassal et al., 1990) (for review see (Seeger and Mason, 2015)) justified its identification as a target in the search for molecules endowed with antiviral activity (Testoni et al., 2017). Based on X-ray crystallography of HBc-NTD derivatives and on cell based assay using mouse hepatocytes cell line a series of HBV assembly inhibitors, also referred to as capsid assembly modulators (CAMs) were identified (Klumpp et al., 2015; Konig et al., 1998; Koschel et al., 1999;

Abbreviations: HBV, hepatitis B virus; eGFP, enhanced green fluorescent protein; TEM, transmission electron microscopy; HBc, hepatitis B core protein; FACS, fluorescence-activated cell sorting; MOA, mechanisms of action; CAMs, capsid assembly modulators; ROI, regions of interest; HAP, heteroaryldihydropyrimidines

* Corresponding author. Morphogenèse et Antigénicité du VIH et des Virus des Hépatites, Inserm – U1259 MAVIVH, Hôpital Bretonneau, 10 boulevard Tonnellé - BP 3223, 37032, Tours Cedex 1, France.
E-mail address: hderocquigny@univ-tours.fr (H. de Rocquigny).

https://doi.org/10.1016/j.antiviral.2019.104557
Received 9 May 2019; Received in revised form 5 July 2019; Accepted 10 July 2019
Available online 11 July 2019

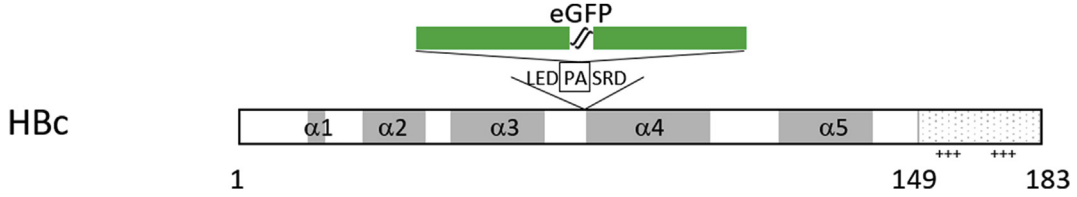

Fig. 1. Diagram of the HBc constructs.
The gray boxes correspond to the helical N-terminal domains of HBc, whereas the dotted box corresponds to the basic C-terminal domain. The fluorescent reporter eGFP is inserted at positions 78 and 80 (Kratz et al., 1999).

Venkatakrishnan and Zlotnick, 2016; Zhou et al., 2017; Campagna et al., 2013). Two classes of CAMs have been defined (Schinazi et al., 2018). The first class groups phenylpropenamide derivatives (PPAs), and sulfamoyl benzamides (SABs) (Berke et al., 2017; Campagna et al., 2013; Corcuera et al., 2018; Feld et al., 2007; Klumpp et al., 2015; Mani et al., 2018). The second class II includes heteroaryldihydropyrimidine (HAPs) (Boucle et al., 2017; Deres et al., 2003). Compounds of both classes reduce pgRNA encapsidation and prevent cccDNA formation (Berke et al., 2017; Boucle et al., 2017; Guo et al., 2017; Lahlali et al., 2018; Lam et al., 2017; Wu et al., 2013; Zhao et al., 2018). However, whereas morphologically intact but empty capsids are formed following treatment with class I molecules, class II molecules induce the production of aberrant capsid polymers *in vitro* (Bourne et al., 2006; Corcuera et al., 2018; Huber et al., 2018; Klumpp et al., 2015; Stray et al., 2005).

Assessments of the antiviral activity of HAP-related compounds in stably HBV-transfected HepAD38 cells or infected HepaRG cells showed that these molecules inhibited HBV replication with an EC_{50} ranging from 50 nM to 200 nM and low cytotoxicity with two-digit micromolar CC50 (Berke et al., 2017; Corcuera et al., 2018; Deres et al., 2003; Huber et al., 2018; Klumpp et al., 2015; Lahlali et al., 2018; Zhou et al., 2017). HAP treatment at 10 fold the EC_{50} for 4–10 days results in an accumulation of large HBc aggregates within the nucleus (Corcuera et al., 2018; Huber et al., 2018; Lahlali et al., 2018).

We describe here the effect on HBc cellular distribution after HAP BAY 41–4109 treatment at 10 times the EC_{50} (0.5–1 μM) for a shorter period (24 h–72 h). We observed aggregate formation, mostly in the cytoplasm, with any large aggregates close to the nucleus enclosed by invaginations of the nuclear envelope. Transmission electron microscopy (TEM) and immuno-TEM also revealed that HBc aggregates corresponded to accumulations of capsid-like shells compressed into an electron-dense material consisting of HBc core fragments, highlighting key differences between BAY 41-4109-mediated HBc aggregates and those obtained *in vitro* with HBc149. Our results shed light on the antiviral mechanisms driven by these molecules and should facilitate comparative studies with other inhibitors of HBV capsid assembly.

2. Materials and methods

2.1. Plasmid DNA

The pTR-UF-HBc183-eGFPopt plasmid encoding a full-length HBc was obtained from Prof. M. Nassal (Kratz et al., 1999). This plasmid encodes a protein in which eGFP, flanked by flexible linkers, replaces amino acids P79 and A80 (Fig. 1) (Kratz et al., 1999; Vogel et al., 2005; Yoo et al., 2012). We obtained pcDNA3-HBc by removing the eGFP sequence from pcDNA-HBc-eGFP with the forward primer GTT-AAC-CTC-GAG-GAT-CCA-GCA-TCT-AGA-GAC-CTG-GTA and the reverse primer TAC-CAG-GTC-TCT-AGA-TGC-TGG-ATC-CTC-GAG-GTT-AAC to re-introduce the ^{79}PA^{80} sequence.

2.2. Cell culture

Experiments were carried out on the Huh7 cell lines. Cells were maintained in Dulbecco's modified Eagle medium (DMEM) supplemented with 10% fetal bovine serum (Gibco, France) and 1% antibiotic mixture (penicillin/streptomycin: Gibco, France) at 37 °C, under an atmosphere containing 5% CO_2. Cells were transfected with jetPEI™ (Life Technologies, Saint Aubin, France).

2.3. Confocal microscopy

We used 2×10^5 Huh7 or HepG2 cells to seed 24-well plates. The cells were transfected with a plasmid encoding HBc. Cells were fixed with 4% paraformaldehyde in PBS, permeabilized with 0.2% Triton/PBS and blocked with 0.4% BSA. The cells were then incubated with a human anti-HBc antibody (Roingeard et al., 1990b), and after washings incubated with Alexa Fluor 488-conjugated goat anti-human antibody (Thermo Fisher Scientific). The last wash contained DAPI and the cells were stored in PBS at 4 °C until observation. Confocal fluorescence micrographs were obtained with a LEICA SP8 gSTED confocal microscope equipped with 63x PL APO 1.40 CS2 Oil (or 40x PL APO 1,30 CS2 Oil), a laser diode at 405 nm for DAPI and an argon laser at 488 nm for Alexa 488. Z-stack images were obtained with LAS X optimized settings. Briefly, images were acquired with 1024 × 1024 pixels in the *x–y* plane, with a pixel size of 150 nm and a step size of 300 nm along the axial axis; we obtained 120–150 images in total, depending on cell thickness (40–50 μm).

2.4. Cell toxicity assay

The cells were treated for 48 h with BAY 41–4109, and a viability test was then performed with 0.5 mg/mL MTT, with detection in a mixture of 0.1% NP40 and 0.067% 6 N HCl in isopropanol. The plate was analyzed with a 630 nm reference filter and a 570 nm test filter. A simultaneous LDH cytotoxicity assay (Pierce LDH Cytotoxicity Assay Kit, Thermo Fisher Scientific) was performed with an associated procedure. Both assays were read with a Dynex MRX TC Revelation Microplate Reader.

2.5. BAY 41–4109 treatment

BAY 41–4109 was synthesized as previously described (Billioud et al., 2011). Six hours after transfection, cells were washed and incubated in 400 μl DMEM, to which we added 4 μl DMSO (1% v/v) or 4 μl of stock solution containing 100 μM BAY 41–4109 in DMSO. The cells were incubated for 24 h, then washed, fixed with PFA and incubated with a specific anti-HBc antibody (Roingeard et al., 1990b). For longer time periods, the medium was refreshed in the same conditions and incubated for an additional 24 h. This protocol is summarized in Figs. 2A and 4A. Dilutions were adapted to obtain 0.1, 0.5 and 5 μM BAY 41–4109, whilst keeping the quantity of DMSO constant (1% v/v).

2.6. Image analysis

We quantitatively analyzed 225 images (3 durations x 5 doses x 15 samples each). All the methods used were implemented in Matlab® 2017b. The images were first pre-processed by wavelet denoising to

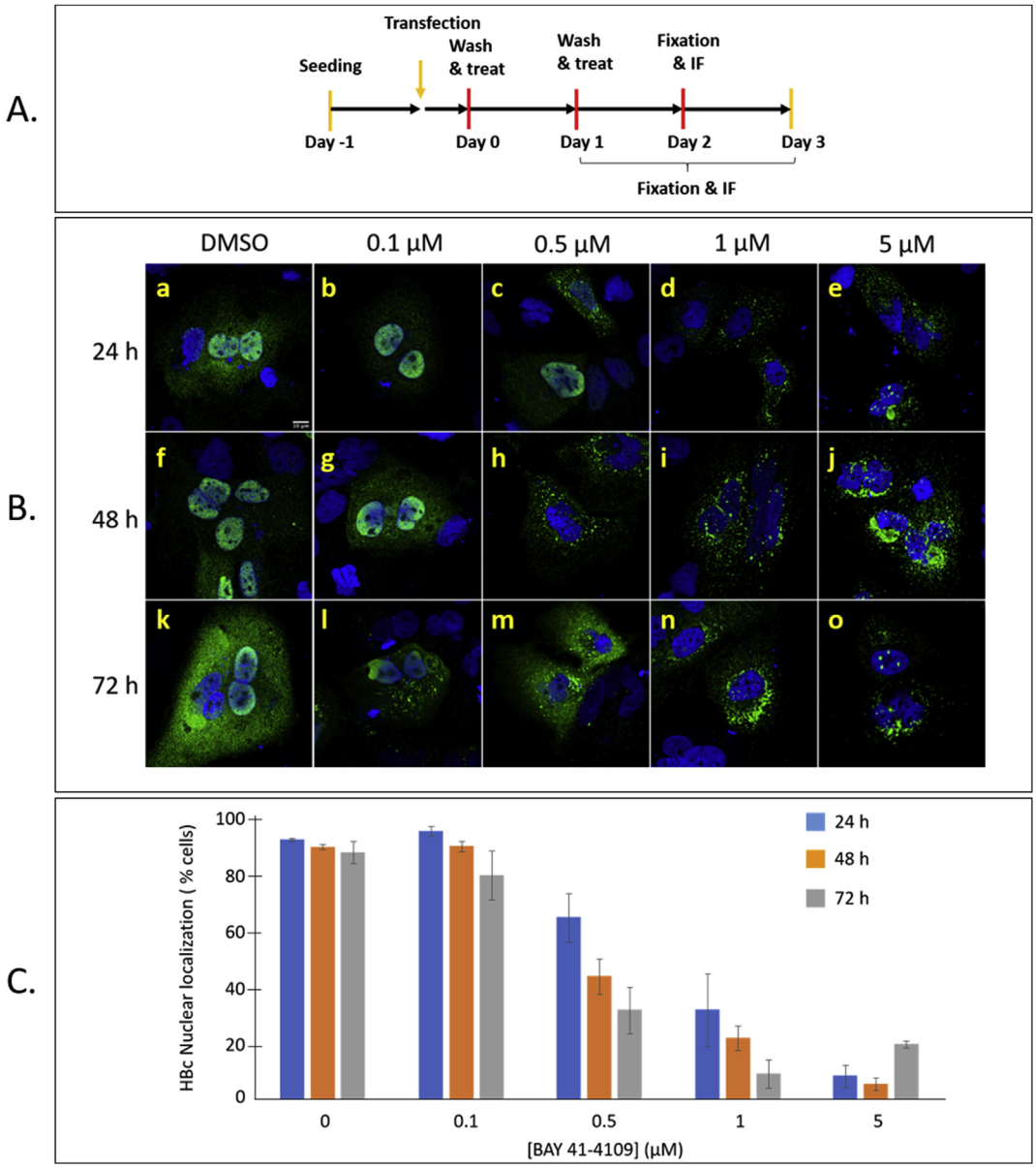

Fig. 2. Immunofluorescence assay on Huh7 cells expressing HBc treated with BAY 41–4109.
A: Diagram of the protocol. Huh7 cells were transfected, the day after plating, with a plasmid encoding HBc. They were then washed 6 h later and various concentrations of BAY 41–4109 were added (day 0). Cells were fixed and stained (day 1, time 24 h) or the medium was refreshed with the same concentration of molecule and the incubation was then stopped at 48 h (day 2) or 72 h (day 3). B: Detection of HBc by immunofluorescence. Cells were fixed, permeabilized and incubated with human anti-HBc antibody. They were thoroughly washed and incubated with anti-human goat antibody labeled with Alexa Fluor 488. Nuclear DNA was counterstained with DAPI and cells were imaged by confocal microscopy. Each image shown corresponds to the merging of the blue- and green-channel images and shows the major phenotype observed. Note that nuclear aggregates appear at higher concentrations or longer incubation times. The white scale bar represents 10 µm. C: Histogram showing the percentage of cells with cytoplasmic fluorescent staining as a function of BAY 41–4109 concentration and incubation time. HBc was observed in the cytoplasm (phenotype: cytoplasm > nucleus) or in the nucleus (phenotype: nucleus > cytoplasm) or was equally distributed between the cytoplasm and the nucleus. This fluorescence distribution was assessed by eye on confocal sections. The percentage of cells with the nucleus > cytoplasm phenotype was calculated by dividing the number of cells with this phenotype by the number of transfected cells and multiplying by 100. Note the progressive decrease in HBc levels in the nucleus with increasing concentration or duration time. Each set of conditions (time and concentration) was performed 3 times, and 80–100 cells were counted per set of conditions. Blue, orange and gray bars correspond to 24 h, 48 h and 72 h, respectively.

improve the signal-to-noise ratio and deconvolved with a regularized Lucy-Richardson approach to improve the separation of real clusters from the background. Images were then binarized with an automatic threshold, and morphological operators were applied to improve the separation of the various aggregates and to eliminate noise and background residuals. Finally, a watershed algorithm was used to detect and label the bright aggregates in the image. The area of each HBc aggregate was measured and converted into the diameter of a disk of equivalent area. Histograms of the percentage of the total area covered by aggregates of different sizes were constructed to represent the size distribution for each set of conditions.

2.7. Transmission electron microscopy

Cells expressing HBc/HBc-eGFP and treated with DMSO or 1 µM BAY 41–4109 for 48 h were sorted and fixed by incubation for 24 h in 4% paraformaldehyde and 1% glutaraldehyde (Sigma, St. Louis, MO) in 0.1 M phosphate buffer (pH 7.2). Samples were washed with PBS and

post-fixed by incubation with 2% osmium tetroxide (Agar Scientific, Stansted, UK) for 1 h. Cells were then fully dehydrated in a graded series of ethanol solutions (70%, 90% and 100%) and propylene oxide (100%). The samples were impregnated with a 1:1 mixture of propylene oxide/Epon resin (Sigma) and then incubated overnight in pure resin. They were then embedded in Epon resin (Sigma) and left to polymerize for 48 h at 60 °C. Ultrathin sections (90 nm) were cut with an EM UC7 ultramicrotome (Leica Microsystems, Wetzlar, Germany). Contrast staining was performed with 2% uranyl acetate (Agar Scientific) and 5% lead citrate (Sigma), and the samples were then observed in a transmission electron microscope (JEOL 1011, Tokyo, Japan).

2.8. Immunogold labeling of ultrathin cryosections by the Tokuyasu method (Tokuyasu, 1973)

Cells expressing HBc/HBc-eGFP and treated with DMSO or with 1 μM BAY 41–4109 for 48 h were sorted and fixed by incubation for 2 h with 4% paraformaldehyde in phosphate buffer (pH 7.6). They were then washed twice with PBS (pH 7.6) and embedded in gelatin (12%). They were infused overnight at 4 °C with 2.3 M sucrose and ultrathin cryosections were then cut at −110 °C on a Leica Microsystems FC7 cryo-ultramicrotome. Sections (80 nm thick) were retrieved in a 1:1 mixture of 2% methylcellulose/2.3 M sucrose and collected on formvar/carbon-coated nickel grids. The gelatin was removed by heating at 37 °C, and the sections were incubated with 1:200 rabbit anti-GFP antibody (ABCAM, ref AB6556) in PBS. The grids were washed six times, for 5 min each, with PBS, and were then incubated with 1:30 gold-conjugated (6 nm particles) goat anti-rabbit (6 nm) antibody in PBS (Aurion, Wageningen, the Netherlands). The grids were washed in PBS (six washes, each lasting 5 min), and rinsed in distilled water. The grids were contrast stained by incubation in a 1:10 mixture of 2% uranyl acetate/2% methylcellulose and viewed in a transmission electron microscope operating at 100 kV (JEOL 1011).

3. Results

3.1. The size and location of BAY 41-4109-induced HBc aggregates depend on time and concentration

The effect of CAMs on HBc aggregation and the cellular localization of these aggregates were unclear and seemed to depend on the class of compound used, its concentration and the duration of treatment (Corcuera et al., 2018; Huber et al., 2018; Nair et al., 2018). We investigated the effect of BAY 41–4109 on HBV capsid morphogenesis in more detail, using Huh7 cells expressing HBc and determining the location and size of the aggregates for various product concentrations and treatment times.

We therefore transfected Huh7 cells with a plasmid encoding HBc alone and incubated them with either DMSO or 0.1–5 μM of BAY 41–4109. Treatment duration was one to three days (Fig. 2A), and the cells were then fixed and stained for HBc with a human polyclonal anti-HBc antibody (Fig. 2B). Consistent with published data (Corcuera et al., 2018; Deroubaix et al., 2015; Sharma et al., 2002; Zhang et al., 2016), we estimated that, 24 h post-transfection and in the absence of BAY 41–4109, ~90% of cells presented punctate HBc staining predominantly localized in the nucleus (Fig. 2B, image a and Fig. 2C, blue bar). This phenotype remained unchanged over periods of 48 h (Fig. 2B, image f and Fig. 2C, orange bar) and 72 h (Fig. 2B, image k and Fig. 2C, gray bar) after transfection. A quantitative analysis of these images revealed that the area covered by the puncta was evenly distributed, small (equivalent to a dot diameter of no more than 0.3 μm, given the lateral diffraction limit (Klar et al., 2000)), and stable over time (Fig. 3, first column). Conversely, both the location and the area of the HBc puncta gradually changed during the incubation of the cells with BAY 41–4109 (0.1 μM, 0.5 μM and 1 μM) for 24–72 h (Fig. 2B, second and third columns). Indeed, the nucleus gradually emptied (Fig. 2C) and image analysis to assess aggregate size revealed a significant number of aggregates with an equivalent diameter of more than 1 μm (Fig. 3, second, third and fourth columns). This result clearly demonstrates the concentration and time dependence of the BAY 41-4109-mediated aggregation of HBc. Consistent with this result, the same phenotype was observed when cells were treated for 24 h with a higher concentration of BAY 41–4109 (5 μM): a large decrease in the nuclear signal (Fig. 2B, first row, Fig. 2C, blue bars) accompanied by the formation of significantly larger puncta in the cytoplasm, with an equivalent diameter of more than 2 μm (Fig. 3, first row). We also investigated various cell types including HepG2 cells expressing HBc alone, Huh7 cells expressing the entire genome, or the HepAD38 cell line that constitutively produce HBV virions. These experiments demonstrated that the BAY 41-0941-mediated purge of the nucleus and formation of cytoplasmic HBc aggregates was independent from the cell type and the replication cycle (Fig. S1).

Taken together, our results show that the size of HBc aggregates (Fig. 3) is clearly correlated with their distribution in the cytoplasm (Fig. 2C).

3.2. Are the nuclear aggregates in the nucleus or at the periphery of the nucleus?

Large aggregates (diameter > 3 μm) were sometimes colocalized with the nucleus when cells expressing HBc were treated with high concentrations of BAY 41–4109 (5 μM) for a longer time period (72 h) (Fig. 2B, last row and Fig. 2C). Given the size of these aggregates, we wondered how such large HBc clusters could localize within the nucleus, given that when Huh7 (or HepAD38) cells are cultured in two-dimensional monolayers, the plated cells contain an oval nucleus with a mean diameter of 10–15 μm (Fig. 2) and a mean height of 3–5 μm (Corcuera et al., 2018; Webster et al., 2009). A *z*-scan acquisition analysis was performed on cells treated with 5 μM BAY 41–4109 for 72 h (Fig. 4). Three regions of interest (ROI) were highlighted on the *x-y* plane of the same cell (red circle) and the *x-z* and *y-z* views of each ROI were enlarged and are reported above (*x-z*) and on the left (y-z) of the image. ROI 1 shows a small HBc aggregate within the nucleus (Fig. 4A) whereas ROI 2 and 3 display larger aggregates inserted into (Fig. 4B) or crossing (Fig. 4C) the entire nucleus. Overall, these images provide evidence that, although small HBc clusters can be found within the nucleus, most, if not all, of the large aggregates are not actually within the nucleus, but are actually in the cytoplasm and at the periphery of nucleus.

3.3. Ultrastructural organization of HBc aggregates in cells, as shown by electron microscopy and immunoelectron microscopy

The effect of CAMs on HBc assembly was investigated *in vitro* by TEM on purified HBc149 from which the basic C-terminal domain was deleted (Huber et al., 2018; Stray et al., 2005; Wu et al., 2013). We investigated the effect of BAY 41–4109 on the HBV capsid shell further by performing TEM and immunoTEM on cells expressing native HBc. These two complementary methods were used to visualize ultrastructural modifications accurately (TEM) and to localize HBc within untreated or BAY 41-4109-treated cells (Immuno-TEM). Cells were therefore transfected with a plasmid expressing HBc together with a plasmid expressing HBc-eGFP (ratio 9:1) and treated for 48 h with 1 μM BAY 41–4109. Cells were sorted by FACS and the pellets obtained were processed for TEM or immuno-TEM.

Immuno-TEM on naïve cells demonstrated the presence of the native capsid (Fig. 5A, enlargements 1–4). Conversely, electron-dense material was easily detected in the cytoplasm of BAY 41-4109-treated cells (Fig. 5B, white arrows) and immuno-TEM confirmed that these structures were strongly positive for HBc protein (Fig. 5B, inset showing intense immunogold labeling for the HBc protein). These large HBc-positive aggregates were never observed in absence of BAY 41–4109

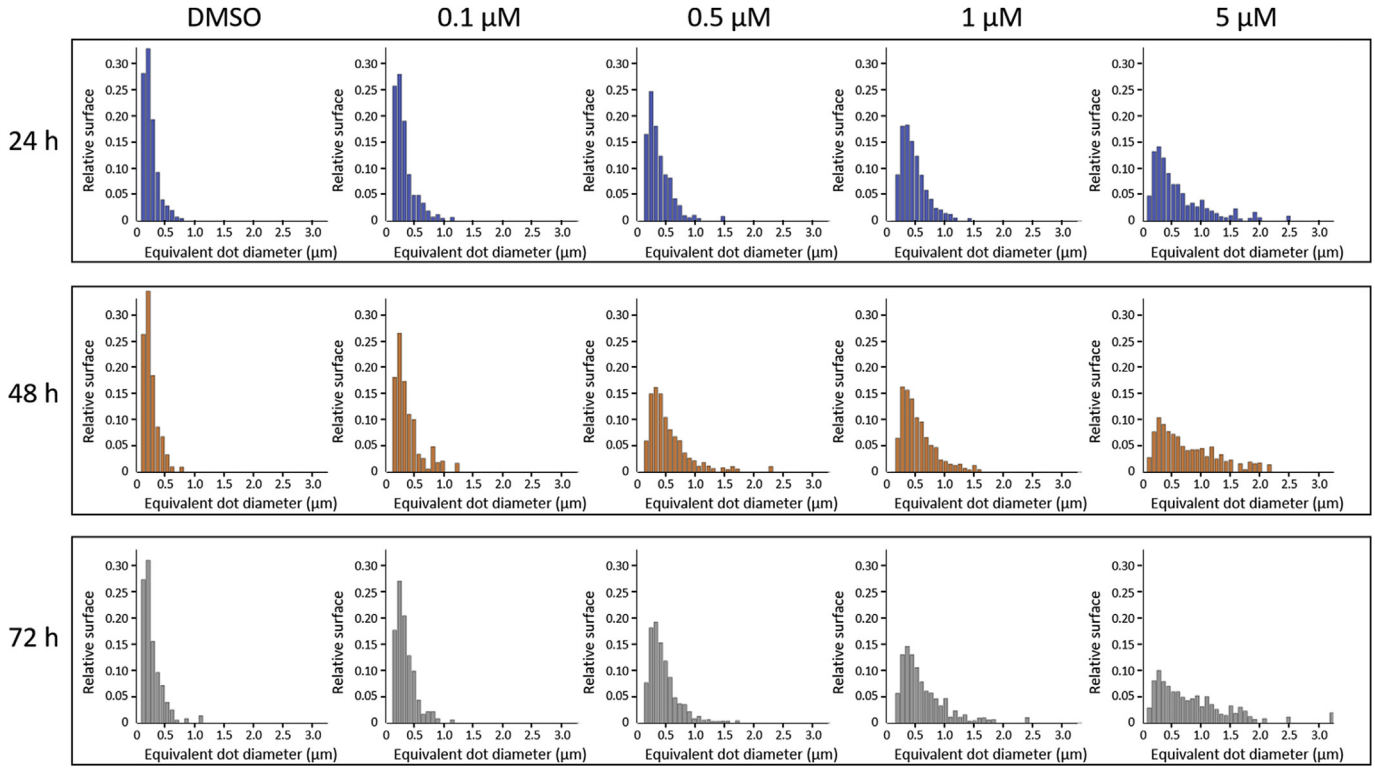

Fig. 3. Distribution of the sizes of HBc aggregates in BAY 41–4109-treated cells.
Each histogram represents a different set of conditions: blue, orange and gray histograms correspond to 24 h, 48 h and 72 h, respectively, and each column represents a different concentration of BAY 41–4109, as indicated at the top of the figure. The total area of each histogram is the same. Each aggregate is detected in the image and its area is converted into the equivalent diameter of a disk of the same area. The smallest areas were ~0.3 µm in diameter, consistent with the diffraction limit (Klar et al., 2000). The *y* axis corresponds to the percentage of the total area covered by aggregates for the given class, whereas the *x* axis corresponds to the disk diameter. Note the progressive shift in size distribution towards larger aggregates with increasing concentration and treatment duration. This analysis was performed on 10–15 images par set of conditions.

treatment, after a careful examination of at least 100 sections of control (DMSO treatment) cells. The large HBc aggregates appeared to be localized within the nucleus on confocal microscopy (Fig. 4), but a precise analysis of their localization by electron microscopy showed them to be mostly cytoplasmic. Electron-dense HBc-positive aggregates were often detected in the perinuclear area, partially surrounded by the nuclear compartment (Fig. 5C and D). These aggregates were actually located in cytoplasmic areas enclosed by invaginations of the nuclear envelope. Nevertheless, in some cases, it was possible to visualize the presence of HBc-positive aggregates within the nuclear compartment (Fig. 5 E1 and 5 E2). To analyze the precise ultrastructure of these aggregates, we then studied the cells by standard TEM (Fig. 6 A). We found that they consisted of amorphous unorganized material (Fig. 6B) mixed with arrays of intact capsid shells arranged edge-to-edge (Fig. 6C and D). Such capsid arrays were never observed in previous EM studies of HBV producing cells (Gerber et al., 1988; Roingeard et al., 1990a; Roingeard and Sureau, 1998) and were not observed in our control (DMSO treatment) cells. On several occasions, a single or double membrane was observed around the electron-dense structures localized in the cytoplasm (Fig. 6, panel B, blue arrows) that could correspond to autophagosome (Lai and Devenish, 2012).

Taken together, these observations suggest that BAY 41–4109 may aggregate preformed capsids tightly together, compressing them into an amorphous protein material.

4. Discussion

The discovery of the three-dimensional structure of HBc paved the way for the development of molecules directed against HBV core protein with a high antiviral potential. We investigated the impact of HAP

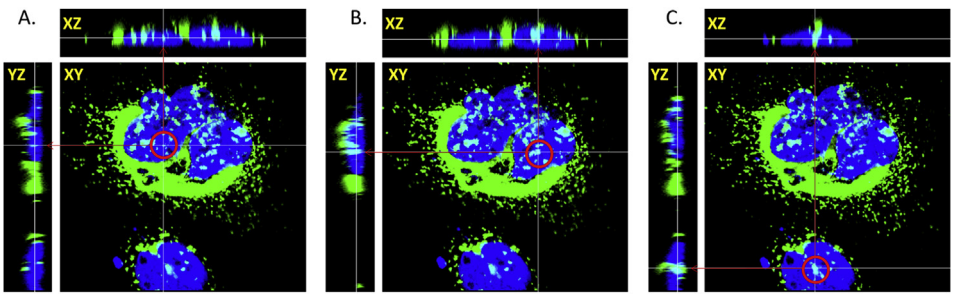

Fig. 4. Examples of *x-z* and *y-z* orthogonal views showing the colocalization of HBc aggregates and the nucleus.
HBc was detected by immunofluorescence staining and the nucleus was counterstained with DAPI. 3D images were obtained by scanning a series of *x-y* planes with axial steps of 300 nm. A, B and C correspond to the *x-y* plane of the same cell and the enlargements of these orthogonal views (*x-z* and *y-z*) are presented above and on the left, respectively. Small HBc aggregates were found within the nucleus, whereas larger HBc aggregates were found at the periphery of the nucleus, probably enclosed in invaginations of the nuclear envelope.

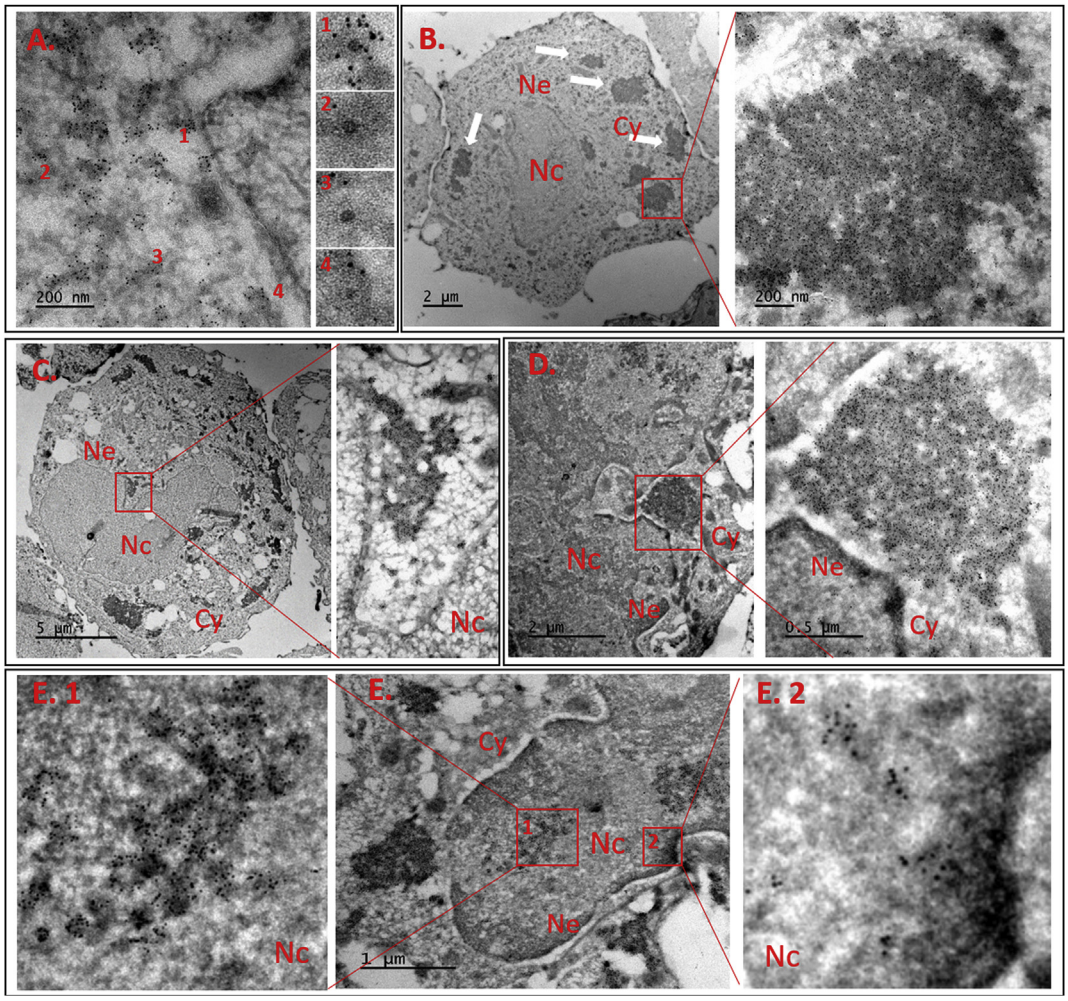

Fig. 5. BAY 41–4109-induced HBc aggregates observed by Immuno-TEM, with the Tokuyasu method.
Huh7 cells were transiently transfected with a mixture of DNA plasmids expressing HBc/HBc-eGFP and incubated with 1 µM BAY 41–4109 for 48 h. After GFP-based sorting, the fixed cells were embedded in gelatin and ultrathin sections were cut and incubated first with rabbit anti-GFP antibody and then with anti-rabbit antibodies conjugated with 6 nm gold particles. A: Huh7 cell expressing HBc/HBc-eGFP and treated with DMSO. Insets 1–4 show various electron-dense particles corresponding to the HBc capsid. B–E: Different examples of Huh7 cells expressing HBc/HBc-eGFP and treated with BAY 41–4109. Nc: Nucleus; Ne: Nuclear envelope; Cy; Cytoplasm.

on HBc in cells, by treating cells expressing HBc with BAY 41–4109 and assessing the intracellular localization and aggregation behavior of HBc. We confirm here that this HAP chemotype induces the formation of large HBc clusters in a time- and dose-dependent manner (Corcuera et al., 2018; Huber et al., 2018; Lahlali et al., 2018; Nair et al., 2018). However, the distribution of these clusters is variable, with accumulation in both the nucleus (Corcuera et al., 2018; Huber et al., 2018; Lahlali et al., 2018) and the cytoplasm ((Nair et al., 2018) and this study, Fig. 2). This heterogeneity of HBc aggregate distribution may be due to the experimental conditions in our study, as we used a low concentration of BAY 41–4109 and a short treatment time. Previous studies also used compounds with the same HAP backbone but surrounded by different chemical groups. Consistent with this hypothesis, structural studies showed that different HAP congeners interact differently with HBc (Klumpp et al., 2015; Zhou et al., 2017), resulting in different effects on capsid structure (Bourne et al., 2006; Katen et al., 2013; Venkatakrishnan et al., 2016). It remains unclear why HBc is found in the nucleus in non-treated cells but aggregates mostly in the cytoplasm in BAY 41-4109-treated cells (Fig. 2). However, the BAY 41–4109-mediated HBc aggregation follows very rapid kinetics (Bourne et al., 2008), such that the cytoplasmic HBc population may aggregate immediately, following the entry of BAY 41–4109 into the cell. In addition, HBc is translated in the cytoplasm (Blondot et al., 2016), where the protein is captured by the aggregation process, which displaces the equilibrium from the nucleus to the cytoplasm. Consequently, BAY 41–4109 may be trapped in cytoplasmic HBc clusters and longer times or higher concentrations may be required to reach the nuclear compartment. Zlotnick and coworkers recently described a fluorescent HAP derivative that was not observed in the nucleus (Nair et al., 2018). For long treatment times and high CAM concentrations, the results of all studies converge (Corcuera et al., 2018; Huber et al., 2018), with the observation of large aggregates mostly, but not exclusively, in the nucleus. However, our study casts doubts on the localization of HBc aggregates within the nucleus. Consistent with the size of the aggregates (2–3 µm; Fig. 3), we found that large HBc clusters were located at the periphery of the nucleus, partly enclosed by invaginations of the nuclear envelope (Figs. 4–6).

We then investigated the structure of HBc clusters. In studies with a purified HBc NTD, HAP derivatives have been shown to divert the assembly of HBc149 lacking the basic C-terminus, resulting in the formation of irregular capsids with open edges associated with large sheet- and tube-like structures (Bourne et al., 2008; Klumpp et al., 2015; Stray et al., 2005; Venkatakrishnan et al., 2016; Zhou et al., 2017). We provide here, for the first time in a cellular context and using the full-length HBc, a very different view of the ultrastructure of the HBc clusters. We observed two main cluster morphologies. The capsids

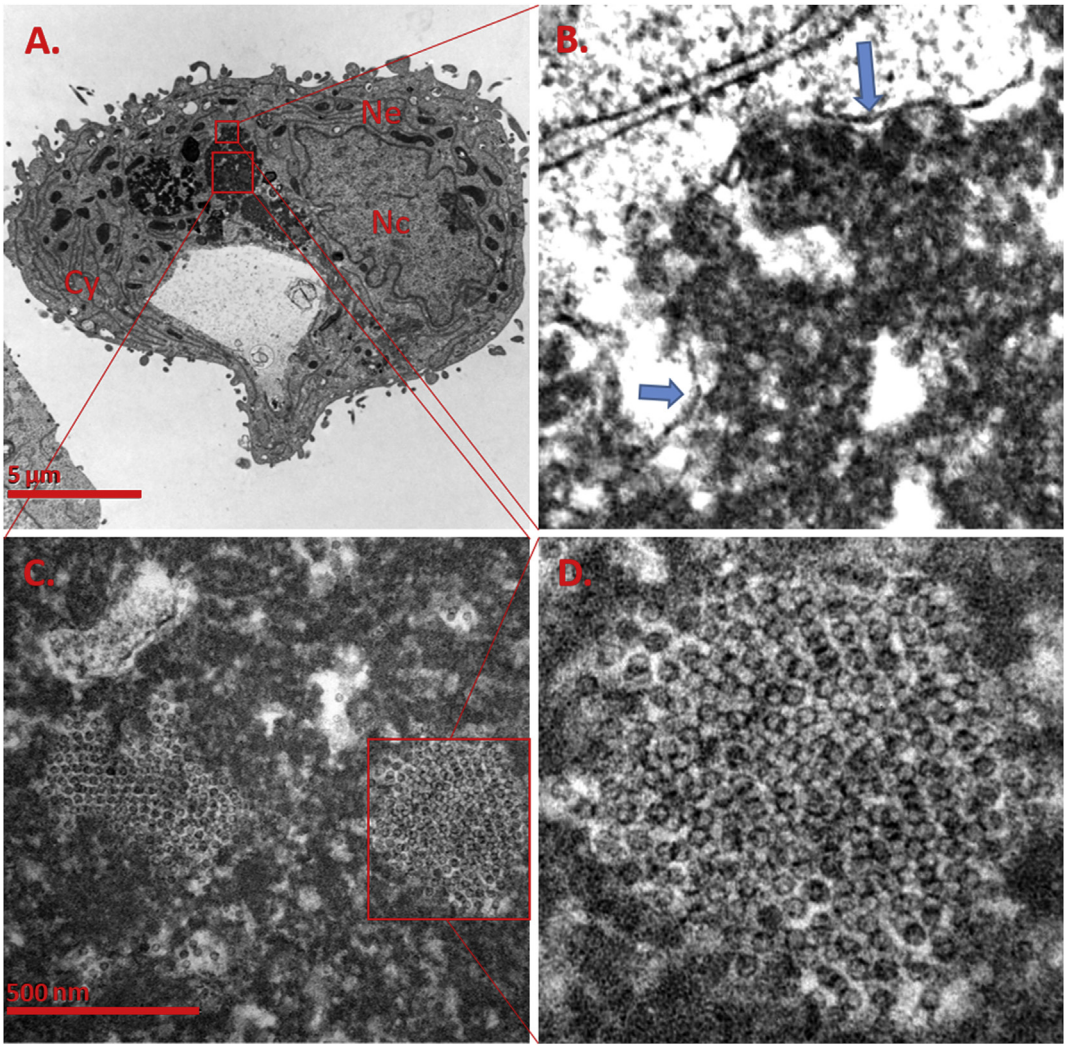

Fig. 6. Electron micrographs of BAY 41–4109-induced HBc aggregates.
Huh7 cells were transiently transfected with a mixture of DNA plasmids expressing HBc/HBc-eGFP and treated with 1 µM BAY 41–4109 for 48 h. The cells were sorted and fixed and ultrathin sections were cut and contrast-stained with uranyl acetate/citrate. A: Typical cell displaying an accumulation of electron-dense cytoplasmic material not observed in control cells. B: Higher magnification of this electron-dense material, probably corresponding to an aggregation of HBc protein. Blue arrows show simple or double membrane potently corresponding to autophagosomes. C: High magnification of the electron-dense material showing regular edge-to-edge layers of HBc capsids (a higher magnification of this area is also shown in D). Note that unorganized aggregated HBc protein is colocalized with intact but condensed HBc capsids in this electron-dense material.

seemed to retain their native form, but rather than being dispersed throughout the cell as single particles, they were aggregated together, sometimes edge-to-edge or in an overlapping manner (Fig. 6 and Fig. S2). These aggregations of intact capsids that were not observed *in vitro* with HBc149 may reflect a different mechanism of BAY 41–4109-mediated HBc misassembly. Indeed, the basic C-terminus may, together with potent cellular partners, participate in HBc assembly kinetics, competing with HAP potency (Ludgate et al., 2016). In the other cluster morphology, an electron-dense structure (Figs. 5 and 6), identified as an amorphous aggregate of core proteins (Fig. 6) was observed. This structure probably corresponds to the aggregation of low-order HBc oligomers trapped in an assembly-deficient state, consistent with the ability of BAY 41–4109 to promote protein-protein interactions (Venkatakrishnan and Zlotnick, 2016). Alternatively, it may correspond to hydrolyzed HBc fragments, consistent with the findings of western-blot analysis (Deres et al., 2003; Huber et al., 2018)). Interestingly, these two aggregate morphologies were mostly associated, in the same electron-dense areas of the cells, suggesting that BAY 41–4109 treatment may cause a compression (and disruption) of the capsid shell to generate this amorphous aggregated protein material. Alternatively, we cannot exclude the possibility that BAY 41–4109 aggregates the unassembled core proteins together with preformed capsid shells, leading to an association of these two different structures in the same areas of the cell.

5. Conclusion

We found that BAY 41–4109 induced HBc aggregation mostly in the cytoplasm and that aggregates formed at the periphery of the nucleus were partially surrounded by invaginations of the nuclear envelope. These HBc aggregates consisted of capsid-like structures aggregated together and mixed with fragments of HBc proteins. Although this molecule is not used clinically, understanding its mechanisms of action will serve as a basis for comparison with other assembly inhibitors currently in development and for some in clinical trials.

Conflicts of interest

None declared.

Acknowledgments

We thank Emmanuelle Blanchard-Laumonnier for fruitful discussions and Jean-Luc Darlix and Julie Sappa for careful reading of the manuscript. We thank M Nassal for plasmids encoding HBc-eGFP. This work was supported by the Agence Nationale de Recherche sur le SIDA et les hépatites virales. We also thank Pierre-Ivan Raynal and Juliette Rousseau from the Electron Microscopy (EM) Facility (IBiSA) of Tours University (http://microscopies.med.univ-tours.fr) for technical support. We thank Cyrille Hoarau from the B Cell Resources (BCR) Facility of Tours University for technical support.

Appendix A. Supplementary data

Supplementary data to this article can be found online at https://doi.org/10.1016/j.antiviral.2019.104557.

References

Berke, J.M., Dehertogh, P., Vergauwen, K., Van Damme, E., Mostmans, W., Vandyck, K., Pauwels, F., 2017. Capsid assembly modulators have a dual mechanism of action in primary human hepatocytes infected with hepatitis B virus. Antimicrob. Agents Chemother. 61. https://doi.org/10.1128/aac.00560-17.

Billioud, G., Pichoud, C., Puerstinger, G., Neyts, J., Zoulim, F., 2011. The main hepatitis B virus (HBV) mutants resistant to nucleoside analogs are susceptible in vitro to non-nucleoside inhibitors of HBV replication. Antivir. Res. 92, 271–276. https://doi.org/10.1016/j.antiviral.2011.08.012.

Blondot, M.L., Bruss, V., Kann, M., 2016. Intracellular transport and egress of hepatitis B virus. J. Hepatol. 64, S49–s59. https://doi.org/10.1016/j.jhep.2016.02.008.

Boucle, S., Lu, X., Bassit, L., Ozturk, T., Russell, O.O., Amblard, F., Coats, S.J., Schinazi, R.F., 2017. Synthesis and antiviral evaluation of novel heteroarylpyrimidines analogs as HBV capsid effectors. Bioorg. Med. Chem. Lett 27, 904–910. https://doi.org/10.1016/j.bmcl.2017.01.010.

Bourne, C., Lee, S., Venkataiah, B., Lee, A., Korba, B., Finn, M.G., Zlotnick, A., 2008. Small-molecule effectors of hepatitis B virus capsid assembly give insight into virus life cycle. J. Virol. 82, 10262–10270. https://doi.org/10.1128/jvi.01360-08.

Bourne, C.R., Finn, M.G., Zlotnick, A., 2006. Global structural changes in hepatitis B virus capsids induced by the assembly effector HAP1. J. Virol. 80, 11055–11061. https://doi.org/10.1128/jvi.00933-06.

Campagna, M.R., Liu, F., Mao, R., Mills, C., Cai, D., Guo, F., Zhao, X., Ye, H., Cuconati, A., Guo, H., Chang, J., Xu, X., Block, T.M., Guo, J.T., 2013. Sulfamoylbenzamide derivatives inhibit the assembly of hepatitis B virus nucleocapsids. J. Virol. 87, 6931–6942. https://doi.org/10.1128/jvi.00582-13.

Chu, T.H., Liou, A.T., Su, P.Y., Wu, H.N., Shih, C., 2014. Nucleic acid chaperone activity associated with the arginine-rich domain of human hepatitis B virus core protein. J. Virol. 88, 2530–2543. https://doi.org/10.1128/JVI.03235-13.

Corcuera, A., Stolle, K., Hillmer, S., Seitz, S., Lee, J.-Y., Bartenschlager, R., Birkmann, A., Urban, A., 2018. Novel non-heteroarylpyrimidine (HAP) capsid assembly modifiers have a different mode of action from HAPs in vitro. Antivir. Res. 158, 135–142. https://doi.org/10.1016/j.antiviral.2018.07.011.

Deres, K., Schroder, C.H., Paessens, A., Goldmann, S., Hacker, H.J., Weber, O., Kramer, T., Niewohner, U., Pleiss, U., Stoltefuss, J., Graef, E., Koletzki, D., Masantschek, R.N., Reimann, A., Jaeger, R., Gross, R., Beckermann, B., Schlemmer, K.H., Haebich, D., Rubsamen-Waigmann, H., 2003. Inhibition of hepatitis B virus replication by drug-induced depletion of nucleocapsids. Science (New York, N.Y.) 299, 893–896. https://doi.org/10.1126/science.1077215.

Deroubaix, A., Osseman, Q., Cassany, A., Begu, D., Rages, J., Kassab, S., Laine, S., Kann, M., 2015. Expression of viral polymerase and phosphorylation of core protein determine core and capsid localization of the human hepatitis B virus. J. Gen. Virol. 96, 183–195. https://doi.org/10.1099/vir.0.064816-0.

Feld, J.J., Colledge, D., Sozzi, V., Edwards, R., Littlejohn, M., Locarnini, S.A., 2007. The phenylpropenamide derivative AT-130 blocks HBV replication at the level of viral RNA packaging. Antivir. Res. 76, 168–177. https://doi.org/10.1016/j.antiviral.2007.06.014.

Gerber, M.A., Sells, M.A., Chen, M.L., Thung, S.N., Tabibzadeh, S.S., Hood, A., Acs, G., 1988. Morphologic, immunohistochemical, and ultrastructural studies of the production of hepatitis B virus in vitro. Labor. Investig. J. Tech. Methods Pathol. 59, 173–180 (https://doi.org/).

Guo, F., Zhao, Q., Sheraz, M., Cheng, J., Qi, Y., Su, Q., Cuconati, A., Wei, L., Du, Y., Li, W., Chang, J., Guo, J.T., 2017. HBV core protein allosteric modulators differentially alter cccDNA biosynthesis from de novo infection and intracellular amplification pathways. PLoS Pathog. 13, e1006658. https://doi.org/10.1371/journal.ppat.1006658.

Huber, A.D., Wolf, J.J., Liu, D., Gres, A.T., Tang, J., Boschert, K.N., Puray-Chavez, M.N., Pineda, D.L., Laughlin, T.G., Coonrod, E.M., Yang, Q., Ji, J., Kirby, K.A., Wang, Z., Sarafianos, S.G., 2018. The heteroaryldihydropyrimidine bay 38-7690 induces hepatitis B virus core protein aggregates associated with promyelocytic leukemia nuclear bodies in infected cells. mSphere 3. https://doi.org/10.1128/mSphereDirect.00131-18.

Katen, S.P., Tan, Z., Chirapu, S.R., Finn, M.G., Zlotnick, A., 2013. Assembly-directed antivirals differentially bind quasiequivalent pockets to modify hepatitis B virus capsid tertiary and quaternary structure. Structure (London, England : 1993) 21, 1406–1416. https://doi.org/10.1016/j.str.2013.06.013.

Klar, T.A., Jakobs, S., Dyba, M., Egner, A., Hell, S.W., 2000. Fluorescence microscopy with diffraction resolution barrier broken by stimulated emission. Proc. Natl. Acad. Sci. U.S.A. 97, 8206–8210 (https://doi.org/).

Klumpp, K., Lam, A.M., Lukacs, C., Vogel, R., Ren, S., Espiritu, C., Baydo, R., Atkins, K., Abendroth, J., Liao, G., Efimov, A., Hartman, G., Flores, O.A., 2015. High-resolution crystal structure of a hepatitis B virus replication inhibitor bound to the viral core protein. Proc. Natl. Acad. Sci. U.S.A. 112, 15196–15201. https://doi.org/10.1073/pnas.1513803112.

Konig, S., Beterams, G., Nassal, M., 1998. Mapping of homologous interaction sites in the hepatitis B virus core protein. J. Virol. 72, 4997–5005 (https://doi.org/).

Koschel, M., Thomssen, R., Bruss, V., 1999. Extensive mutagenesis of the hepatitis B virus core gene and mapping of mutations that allow capsid formation. J. Virol. 73, 2153–2160 (https://doi.org/).

Kratz, P.A., Bottcher, B., Nassal, M., 1999. Native display of complete foreign protein domains on the surface of hepatitis B virus capsids. Proc. Natl. Acad. Sci. U.S.A. 96, 1915–1920 (https://doi.org/).

Ladner, S.K., Otto, M.J., Barker, C.S., Zaifert, K., Wang, G.H., Guo, J.T., Seeger, C., King, R.W., 1997. Inducible expression of human hepatitis B virus (HBV) in stably transfected hepatoblastoma cells: a novel system for screening potential inhibitors of HBV replication. Antimicrob. Agents Chemother. 41, 1715–1720 (https://doi.org/).

Lahlali, T., Berke, J.M., Vergauwen, K., Foca, A., Vandyck, K., Pauwels, F., Zoulim, F., Durantel, D., 2018. Novel Potent Capsid Assembly Modulators Regulate Multiple Steps of the Hepatitis B Virus Life-Cycle. Antimicrobial Agents and Chemotherapy. https://doi.org/10.1128/aac.00835-18.

Lai, S.C., Devenish, R.J., 2012. LC3-Associated phagocytosis (LAP): connections with host autophagy. Cells 1, 396–408. https://doi.org/10.3390/cells1030396.

Lam, A.M., Ren, S., Espiritu, C., Kelly, M., Lau, V., Zheng, L., Hartman, G.D., Flores, O.A., Klumpp, K., 2017. Hepatitis B virus capsid assembly modulators, but not nucleoside analogs, inhibit the production of extracellular pregenomic RNA and spliced RNA variants. Antimicrob. Agents Chemother. 61. https://doi.org/10.1128/aac.00680-17.

Liang, T.J., Block, T.M., McMahon, B.J., Ghany, M.G., Urban, S., Guo, J.T., Locarnini, S., Zoulim, F., Chang, K.M., Lok, A.S., 2015. Present and future therapies of hepatitis B: from discovery to cure. Hepatology (Baltimore, Md.) 62, 1893–1908. https://doi.org/10.1002/hep.28025.

Ludgate, L., Liu, K., Luckenbaugh, L., Streck, N., Eng, S., Voitenleitner, C., Delaney, W.E.t., Hu, J., 2016. Cell-free hepatitis B virus capsid assembly dependent on the core protein C-terminal domain and regulated by phosphorylation. J. Virol. 90, 5830–5844. https://doi.org/10.1128/jvi.00394-16.

Mani, N., Cole, A.G., Phelps, J.R., Ardzinski, A., Cobarrubias, K.D., Cuconati, A., Dorsey, B.D., Evangelista, E., Fan, K., Guo, F., Guo, H., Guo, J.T., Harasym, T.O., Kadhim, S., Kultgen, S.G., Lee, A.C.H., Li, A.H.L., Long, Q., Majeski, S.A., Mao, R., McClintock, K.D., Reid, S.P., Rijnbrand, R., Snead, N.M., Micolochick Steuer, H.M., Stever, K., Tang, S., Wang, X., Zhao, Q., Sofia, M.J., 2018. Preclinical profile of AB-423, an inhibitor of hepatitis B virus pregenomic RNA encapsidation. Antimicrob. Agents Chemother. 62. https://doi.org/10.1128/aac.00082-18.

Nair, S., Li, L., Francis, S., Turner, W.W., VanNieuwenhze, M., Zlotnick, A., 2018. Use of a fluorescent analogue of a HBV core protein-directed drug to interrogate an antiviral mechanism. J. Am. Chem. Soc. 140, 15261–15269. https://doi.org/10.1021/jacs.8b07988.

Nassal, M., Junker-Niepmann, M., Schaller, H., 1990. Translational inactivation of RNA function: discrimination against a subset of genomic transcripts during HBV nucleocapsid assembly. Cell 63, 1357–1363 (https://doi.org/).

Neuveut, C., Wei, Y., Buendia, M.A., 2010. Mechanisms of HBV-related hepatocarcinogenesis. J. Hepatol. 52, 594–604. https://doi.org/10.1016/j.jhep.2009.10.033.

Piver, E., Boyer, A., Gaillard, J., Bull, A., Beaumont, E., Roingeard, P., Meunier, J.C., 2017. Ultrastructural organisation of HCV from the bloodstream of infected patients revealed by electron microscopy after specific immunocapture. Gut 66, 1487–1495. https://doi.org/10.1136/gutjnl-2016-311726.

Roingeard, P., Lu, S.L., Sureau, C., Freschlin, M., Arbeille, B., Essex, M., Romet-Lemonne, J.L., 1990a. Immunocytochemical and electron microscopic study of hepatitis B virus antigen and complete particle production in hepatitis B virus DNA transfected HepG2 cells. Hepatology (Baltimore, Md 11, 277–285 (https://doi.org/).

Roingeard, P., Romet-Lemonne, J.L., Leturcq, D., Goudeau, A., Essex, M., 1990b. Hepatitis B virus core antigen (HBc Ag) accumulation in an HBV nonproducer clone of HepG2-transfected cells is associated with cytopathic effect. Virology 179, 113–120 (https://doi.org/).

Roingeard, P., Sureau, C., 1998. Ultrastructural analysis of hepatitis B virus in HepG2-transfected cells with special emphasis on subviral filament morphogenesis. Hepatology (Baltimore, Md 28, 1128–1133. https://doi.org/10.1002/hep.510280431.

Schinazi, R.F., Ehteshami, M., Bassit, L., Asselah, T., 2018. Towards HBV curative therapies. Liver Int. : Off. J. Int. Assoc. Study Liver 38 (Suppl. 1), 102–114. https://doi.org/10.1111/liv.13656.

Seeger, C., Mason, W.S., 2015. Molecular biology of hepatitis B virus infection. Virology 479–480, 672–686. https://doi.org/10.1016/j.virol.2015.02.031.

Sharma, R.R., Dhiman, R.K., Chawla, Y., Vasistha, R.K., 2002. Immunohistochemistry for core and surface antigens in chronic hepatitis. Trop. Gastroenterol. : Off. J. Digest. Dis. Found. 23, 16–19 (https://doi.org/).

Stray, S.J., Bourne, C.R., Punna, S., Lewis, W.G., Finn, M.G., Zlotnick, A., 2005. A heteroaryldihydropyrimidine activates and can misdirect hepatitis B virus capsid assembly. Proc. Natl. Acad. Sci. U.S.A. 102, 8138–8143. https://doi.org/10.1073/pnas.0409732102.

Testoni, B., Durantel, D., Zoulim, F., 2017. Novel targets for hepatitis B virus therapy.

Liver Int. : Off. J. Int. Assoc. Study Liver 37 (Suppl. 1), 33–39. https://doi.org/10.1111/liv.13307.

Tokuyasu, K.T., 1973. A technique for ultracryotomy of cell suspensions and tissues. J. Cell Biol. 57, 551–565 (https://doi.org/).

Venkatakrishnan, B., Katen, S.P., Francis, S., Chirapu, S., Finn, M.G., Zlotnick, A., 2016. Hepatitis B virus capsids have diverse structural responses to small-molecule ligands bound to the heteroaryldihydropyrimidine pocket. J. Virol. 90, 3994–4004. https://doi.org/10.1128/jvi.03058-15.

Venkatakrishnan, B., Zlotnick, A., 2016. The structural biology of hepatitis B virus: form and function. Ann. Rev. Virol. 3, 429–451. https://doi.org/10.1146/annurev-virology-110615-042238.

Vogel, M., Vorreiter, J., Nassal, M., 2005. Quaternary structure is critical for protein display on capsid-like particles (CLPs): efficient generation of hepatitis B virus CLPs presenting monomeric but not dimeric and tetrameric fluorescent proteins. Proteins 58, 478–488. https://doi.org/10.1002/prot.20312.

Webster, M., Witkin, K.L., Cohen-Fix, O., 2009. Sizing up the nucleus: nuclear shape, size and nuclear-envelope assembly. J. Cell Sci. 122, 1477–1486. https://doi.org/10.1242/jcs.037333.

Wu, G., Liu, B., Zhang, Y., Li, J., Arzumanyan, A., Clayton, M.M., Schinazi, R.F., Wang, Z., Goldmann, S., Ren, Q., Zhang, F., Feitelson, M.A., 2013. Preclinical characterization of GLS4, an inhibitor of hepatitis B virus core particle assembly. Antimicrob. Agents Chemother. 57, 5344–5354. https://doi.org/10.1128/aac.01091-13.

Yoo, L., Park, J.S., Kwon, K.C., Kim, S.E., Jin, X., Kim, H., Lee, J., 2012. Fluorescent viral nanoparticles with stable in vitro and in vivo activity. Biomaterials 33, 6194–6200. https://doi.org/10.1016/j.biomaterials.2012.05.028.

Zhang, X., Lu, W., Zheng, Y., Wang, W., Bai, L., Chen, L., Feng, Y., Zhang, Z., Yuan, Z., 2016. In situ analysis of intrahepatic virological events in chronic hepatitis B virus infection. J. Clin. Investig. 126, 1079–1092. https://doi.org/10.1172/jci83339.

Zhao, Q., Hu, Z., Cheng, J., Wu, S., Luo, Y., Chang, J., Hu, J., Guo, J.T., 2018. Hepatitis B virus core protein dephosphorylation occurs during pregenomic RNA encapsidation. J. Virol. 92. https://doi.org/10.1128/jvi.02139-17.

Zhou, Z., Hu, T., Zhou, X., Wildum, S., Garcia-Alcalde, F., Xu, Z., Wu, D., Mao, Y., Tian, X., Zhou, Y., Shen, F., Zhang, Z., Tang, G., Najera, I., Yang, G., Shen, H.C., Young, J.A., Qin, N., 2017. Heteroaryldihydropyrimidine (HAP) and sulfamoylbenzamide (SBA) inhibit hepatitis B virus replication by different molecular mechanisms. Sci. Rep. 7, 42374. https://doi.org/10.1038/srep42374.